Genome Medicine

RESEARCH

Open Access

A novel transcriptional signature identifies T-cell infiltration in high-risk paediatric cancer

Chelsea Mayoh[1,2,3], Andrew J. Gifford[1,2,4], Rachael Terry[1,2], Loretta M. S. Lau[1,2,5], Marie Wong[1,2], Padmashree Rao[1], Tyler Shai-Hee[1], Federica Saletta[1], Dong-Anh Khuong-Quang[6,7], Vicky Qin[8,9], Marion K. Mateos[1,2,5], Deborah Meyran[8,9], Katherine E. Miller[10,11], Aysen Yuksel[12], Emily V. A. Mould[1], Rachel Bowen-James[1,13,14], Dinisha Govender[15], Akanksha Senapati[5], Nataliya Zhukova[16,17,18], Natacha Omer[19,20], Hetal Dholaria[21,22], Frank Alvaro[23], Heather Tapp[24], Yonatan Diamond[5,6], Luciano Dalla Pozza[15], Andrew S. Moore[19,25], Wayne Nicholls[19,26], Nicholas G. Gottardo[21,22], Geoffrey McCowage[15], Jordan R. Hansford[24,27], Seong-Lin Khaw[6,7], Paul J. Wood[16,17,18], Daniel Catchpoole[12], Catherine E. Cottrell[10,11,28], Elaine R. Mardis[10,11,29], Glenn M. Marshall[1,2,5], Vanessa Tyrrell[1,2], Michelle Haber[1,2], David S. Ziegler[1,2,5], Orazio Vittorio[1,2], Joseph A. Trapani[8,9], Mark J. Cowley[1,2], Paul J. Neeson[8,9] and Paul G. Ekert[1,2,7,8,9*]

Abstract

Background Molecular profiling of the tumour immune microenvironment (TIME) has enabled the rational choice of immunotherapies in some adult cancers. In contrast, the TIME of paediatric cancers is relatively unexplored. We speculated that a more refined appreciation of the TIME in childhood cancers, rather than a reliance on commonly used biomarkers such as tumour mutation burden (TMB), neoantigen load and PD-L1 expression, is an essential prerequisite for improved immunotherapies in childhood solid cancers.

Methods We combined immunohistochemistry (IHC) with RNA sequencing and whole-genome sequencing across a diverse spectrum of high-risk paediatric cancers to develop an alternative, expression-based signature associated with $CD8^+$ T-cell infiltration of the TIME. Furthermore, we explored transcriptional features of immune archetypes and T-cell receptor sequencing diversity, assessed the relationship between $CD8^+$ and $CD4^+$ abundance by IHC and deconvolution predictions and assessed the common adult biomarkers such as neoantigen load and TMB.

Results A novel 15-gene immune signature, Immune Paediatric Signature Score (IPASS), was identified. Using this signature, we estimate up to 31% of high-risk cancers harbour infiltrating T-cells. In addition, we showed that PD-L1 protein expression is poorly correlated with PD-L1 RNA expression and TMB and neoantigen load are not predictive of T-cell infiltration in paediatrics. Furthermore, deconvolution algorithms are only weakly correlated with IHC measurements of T-cells.

Conclusions Our data provides new insights into the variable immune-suppressive mechanisms dampening responses in paediatric solid cancers. Effective immune-based interventions in high-risk paediatric cancer will require individualised analysis of the TIME.

*Correspondence:
Paul G. Ekert
pekert@ccia.org.au
Full list of author information is available at the end of the article

Keywords Paediatric cancer, Tumour immune microenvironment, T-cell infiltration, Biomarkers, Transcriptome signature

Background

The comprehensive genomic analysis of paediatric cancer has provided a wealth of new insights into the distinct molecular nature of childhood cancers. The primary goals of many genomics studies of childhood cancers have focused on the identification of therapeutic options encoded in the genome of cancer cells that would otherwise go unrecognised. Studies such as ZERO Childhood Cancer [1], INFORM [2] and the Pediatric Cancer Genome Project [3] have shown that this can translate into improved patient outcomes. However, the genomic data also includes information about the makeup of the tumour microenvironment, since the RNA of infiltrating immune cells, stromal and vascular cells are also sequenced.

The importance of deciphering the tumour immune microenvironment (TIME) has been driven by the extraordinary impact on the treatment of melanoma, lung adenocarcinoma and head and neck cancers [4] of agents (typically recombinant antibodies) that inhibit with immune checkpoint molecules such as programmed cell death 1 (PD1), its ligand PD1 ligand 1 (PD-L1) or cytotoxic T lymphocyte antigen 4 (CTLA-4), all of which downregulate T-cell activation [5, 6]. TIME and tumour-intrinsic features, such as PD-L1 expression, high tumour mutation burdens (TMB) and high neoantigen load increase the potential for an anti-tumour T-cell response following anti-PD-1 treatment [7]. Evidence also suggests that a more diverse T-cell receptor repertoire is associated with improved response to anti-PD-1 [8, 9]. However, whilst such biomarkers are applied in some paediatric cancer trials, there is limited evidence to support their validity, and most children with cancer are not responsive to immunotherapy [10–13]. This suggests strongly that the microenvironment of childhood cancers is distinct from common adult cancers, and successful immune therapies will require a better understanding of the make-up of the immune microenvironment in childhood cancer types.

The TIME comprises a diverse range of $CD45^+$ leucocytes, collectively called tumour infiltrating leucocytes (TILs), which includes $CD4^+$ and $CD8^+$ T-cells, B-cells, tumour-associated macrophages, dendritic cells, myeloid-derived suppressor cells and natural killer cells. The TIME can be classified as 'immune-inflamed' with infiltrating T-cells, 'immune-excluded' where T-cells are present but confined to the tumour periphery, or 'immune-desert' which denotes the total absence of T-cells [14]. Immunohistochemistry is the most established and direct methodology to detect the presence of immune cells in a tumour and to assess the relationship between immune and tumour cells. However, RNA sequencing (RNA-seq) is increasingly used to identify immune cell subsets in a tumour and to infer from gene expression profiles the probable nature of the TIME.

Clinical data from immunotherapy trials in adult cancers indicates that T-cell inflamed tumours are more responsive, and this has been a driver to develop multiple different expression-based signatures to detect and characterise TILs [15–19]. Algorithms such as CIBERSORTx (CSX), quanTIseq and MCP-counter use the expression of key genes to infer the immune cell composition of the TIME from bulk RNA-seq data [20–24]. In contrast to adult cancers, TMB, PD-L1 expression, TIL signatures and deconvolution algorithms have not been systematically applied in paediatric cancers to predict tumour T-cell inflammation. Therefore, a key unmet challenge is identifying the molecular features of paediatric cancers which most accurately characterise the TIME. Two such biomarkers, TMB and PD-L1 expression, appear to be less relevant in the paediatric setting than in adult cancers, with the exception of rare hypermutated tumours harbouring a DNA mismatch repair deficiency or polymerase proofreading deficiency. Whilst hypermutated tumours have been shown to respond to immunotherapy [25], most paediatric tumours have an order of magnitude fewer mutations than adult cancers [1, 26]. PD-L1 expression is reportedly low across paediatric tumour subtypes, and the correlation between transcript levels and protein expression is not well established [27, 28].

We have undertaken a comprehensive characterisation of T-cell infiltration in a diverse spectrum of high-risk paediatric cancers, combining IHC, RNA-seq and whole-genome sequencing (WGS). We have cross-referenced the genomic and RNA-seq data with $CD8^+$ and $CD4^+$ IHC staining on the same tumour specimens to define and validate a novel paediatric-specific gene signature that identifies tumours infiltrated by $CD8^+$ T-cells. Moreover, we explored the relationship between the gene signature we identified and transcriptional features associated with distinct immune archetypes, providing a unique and detailed insight into the molecular features of the immune landscape across a broad range of paediatric cancers. We also show that PD-L1 RNA expression correlated poorly with PD-L1

protein expression and that commonly used deconvolution algorithms had only weak correlations with IHC-determined measures of T-cell infiltration. We propose that our novel signature provides a unique and more accurate identification of T-cell infiltrated paediatric cancers.

Methods

Patients and samples

This is a retrospective analysis of the tumour immune microenvironment from 347 patient samples that were obtained as part of the Australian ZERO Childhood Cancer Precision Medicine Program consisting of the TARGET and PRISM clinical trials. The TARGET pilot study recruited patients from the two children's hospitals in Sydney (Sydney Children's Hospital, Randwick, and the Children's Hospital at Westmead), Australia, from June 2015 to October 2017 and was approved by the Sydney Children's Hospitals Network Human Research Ethics Committee (LNR/14/SCH/497), with the results of the pilot study already published [29]. The PRISM clinical trial (NCT03336931) data for this analysis was collected from September 2017 to August 2020 at all eight paediatric oncology centres around Australia (Sydney Children's Hospital, Randwick; the Children's Hospital at Westmead, Sydney; Queensland Children's Hospital, Brisbane; Perth Children's Hospital, Perth; Women's & Children's Hospital, Adelaide; John Hunter Hospital, Newcastle; Royal Children's Hospital, Melbourne; and Monash Children's Hospital, Melbourne) and was approved by the Hunter New England Human Research Ethics Committee of the Hunter New England Local Health District (reference no. 17/02/015/4.06) and the New South Wales Human Research Ethics Committee (reference no. HREC/17/HNE/29). The PRecISion Medicine for Children With Cancer (PRISM) clinical trial is a multicentre prospective study of the feasibility and clinical value of a diagnostic service for identifying therapeutic targets and recommending personalised treatment for children and adolescents with high-risk cancer (Additional file 1: Fig. S1). The clinical trial enrolled the first patient on 22 September 2017 and is currently ongoing. Patients are eligible if they are 21 years of age and under, deemed to have a high-risk paediatric cancer with less than 30% chance of survival, life expectancy greater than 6 weeks and appropriate tissue samples available for analysis. The primary outcome of PRISM is to assess the proportion of patients for whom a personalised medicine recommendation can be made using a comprehensive diagnostic platform within a clinically relevant timeframe. Secondary outcomes are to assess the proportion of tumour samples found to have actionable molecular alterations, proportion of tumours where in vitro high-throughput drug screening and in vivo drug sensitivity testing can be successfully performed, proportion undergoing in vitro and in vivo drug screening where a potential treatment option is identified, the number of weeks from enrolment to a report being issued to the treating clinician, proportion of patients who subsequently receive the recommended personalised therapy and the description of the barriers or reason for patients not receiving the recommended personalised therapy. Informed consent was received for each patient enrolled on the clinical trial.

Data from 347 patients enrolled on either the TARGET pilot study [29] or the PRISM clinical trial are included in this analysis, of which the molecular landscape of the 228 patients enrolled up until June 2019 has been previously described by Wong et al. [1]. The additional 119 samples were from patients subsequently enrolled on PRISM between July 2019 and August 2020. Of the 347 patient samples, 78 tumour tissue sections were obtained from all patients where sufficient tissue block material was available to perform immune cell-specific IHC analysis. To perform a validation of the IPASS, an additional 57 patients with RNA-seq data were recruited onto PRISM after the IPASS was developed and were enrolled between August 2020 and February 2021, called the internal validation cohort. Of these 57 patients, 15 had tumour tissue sections available for IHC. An external validation dataset was also acquired from the Institute for Genomic Medicine at Nationwide Children's Hospital (NCH; Columbus, OH, USA) for 64 extracranial tumours with RNA-seq data, of which 11 had tumour sections for IHC. Patients at NCH were previously enrolled on an IRB-approved translational research protocol (IRB17-00,206), which included exome- and RNA-seq of frozen tumour as well as banking of additional paraffin-embedded tissue blocks.

Sequencing analysis

RNA-seq and whole-genome sequencing were conducted on all ZERO samples, with data processing and analysis as described in Wong et al. [1]. In brief, the 64 samples received from NCH, the RNA-seq libraries were constructed following DNase treatment and ribosomal transcript depletion of total RNA extracts, using the NEBNext® Ultra™ II Directional RNA Library Prep Kit for Illumina (New England Biolabs Inc., Ipswich, MA, USA), according to the manufacturer's instructions. Sequencing was performed on either Illumina HiSeq 4000 or NovaSeq 6000 to generate paired 151 base-pair reads, followed by alignment to the GRCh38 reference genome. Transcripts per million (TPM) values were generated from aligned paired-end RNA sequence data using Salmon with bootstrapping set to 100 [30].

Immunohistochemistry

We obtained 78 tumour tissue sections from paraffin-embedded blocks of patients with high-risk CNS or extracranial tumours for IHC. We received an additional 15 tissue sections from ZERO and 11 from Nationwide Children's Hospital (NCH) to perform CD8 IHC as a validation cohort. Tissue sections were stained with CD45 (EP322Y, ab40763), CD8 (ab4055), CD4 (EPR6855, ab133616) at a 1:500 dilution and PD-L1 (rabbit monoclonal anit-PD-L1 primary antibody; Cell Signaling Technology, clone: E1L3N, CAT#13,684) at a 1:200 dilution on the Leica BOND RX. Human tonsil was used as the positive control for staining, as well as the negative control (secondary antibody only). Tumours were classified as PD-L1 positive if $\geq 1\%$ of total cells displayed positive membranous staining as described previously [31]. Cytoplastic staining of PD-L1 was also detected; however, these cells were not classified as PD-L1-positive tumour cells. CD45, CD8 and CD4 slides were scanned on the Aperio Scanscope XT and analysed using the QuPath [32] software to analyse the number (per mm2) of positive cells in the entire tumour section. Immunohistochemical staining for CD4 and CD8 was further qualitatively assessed by a paediatric pathologist (AJG) using a standard light microscope, blinded to the molecularly determined immune status of the tumour. An accompanying H&E-stained slide was available for review for most cases. Tumours were classified as immune 'cold', 'altered' or 'hot' as previously published [15]. There were few or absent CD4/CD8-positive T-cells in 'cold' tumours; more widespread T-cells in 'hot' tumours; whilst 'altered' tumours contained either a moderate number of T-cells within the tumour or T-cells at the tumour periphery with absent intratumoural staining.

Deconvolution algorithms

CIBERSORTx [21] deconvolution algorithm was performed on the TPM expression matrix derived from RNA-seq data on 347 samples. The 'impute cell fractions' job mode was run in both absolute and relative mode against the LM22 signature [20]. The analysis was done in B mode for batch correction, quantile normalisation was disabled and 500 permutations performed. The deconvolution module of quanTIseq [22] was performed on the pre-computed expression matrix (beginning at quanTIseq step 3) with –tumor = TRUE and –method = lsei where deconvolution was performed against 10 immune cell types and the fraction of uncharacterised cells identified. MCP-counter (v1.1) [23] R package was run on the gene expression matrix to identify 8 immune cell populations, endothelial cells and fibroblasts.

Development of the novel paediatric signature

The Immune Paediatric Signature Score (IPASS) was developed using a random forest machine learning approach. Using the IHC classifications, we combined the hot and altered together to form an immune-inflamed group. The cohort was randomly assigned into a training set ($N=34$) and a test set ($N=35$), with equal proportions of immune-inflamed and -cold in each set. We obtained the expression profile for the training set and filtered for the 766 immune-specific genes present in the NanoString immune profiling panel [33]. The classifier was developed using the R packages caret [34] and randomForest [35]. We then extracted those genes from the classifier ($n=15$ genes) based on the highest GINI values. We converted this signature into an Immune Paediatric Signature Score (IPASS) by calculating the average sum of the log-transformed TPM values for the 15 genes in the signature. Using the entire cohort ($N=291$), we then normalised the IPASS to obtain a score between -1 and 1. In the results, we describe the performance of IPASS using a normalised threshold of ≥ -0.25, which corresponds to a non-normalised threshold of ≥ 0.83 to classify samples as T-cell infiltrated.

T-cell receptor sequencing

For the identification of T-cell clones, we used MiXCR (v3.0.13) [36] on bulk RNA-seq data using default parameters. Filtering and QC were performed within MiXCR and only clonotypes associated with TCR beta were extracted and used in the analysis. The total number of clones, total number of reads and proportions of each clone were assessed for all CNS and extracranial tumours.

Neoepitope prediction

OptiType (v1.3.3) [37] was performed on germline paired-end whole-genome sequencing fastq files after fishing for HLA reads at 95% identity, taking only the top match with razers3 (v3.5.8) [38] (razers3 -i95 -m 1 -dr 0) to identify HLA types. Each end was filtered separately before running OptiType with default parameters for paired-end sequences. Somatic variant calls annotated with VEP were combined with the HLA typing for each patient and analysed through pVACseq [39] using NetMHCcons [40] for identifying the binding of candidate neoantigens for each HLA type. A mutant peptide was considered for each neoepitope if the mutant peptide had an IC_{50} binding affinity <500 nM, the wild-type peptide had an IC_{50} binding affinity >500 nM and was expressed in RNA-seq (TPM >1). Each mutation resulting in a predicted neoepitope was considered as only one neoantigen regardless of the number of

predicted neoepitopes. The total number of neoantigens for all CNS and extracranial tumours was assessed.

Immune gene expression

We sought to explore the expression of a selected list of immune checkpoint and regulatory genes (Additional file 1: Table S1) and assess the relationship to IPASS. We performed unsupervised hierarchical *K*-means clustering to identify specific groupings of immune genes where their expression profiles were most correlated with IPASS.

Immune archetype classification

For deeper immune classification, we applied the dominant immune archetypes as defined in Combes et al. and followed the gene signature score methods described in the paper [41]. In brief, we downloaded the 12-gene signatures supplied in their supplementary tables and ran the get_score.py function from the papers associated GitHub page (https://github.com/UCSF-DSCOLAB/pan_cancer_immune_archetypes). This calculated a score for each sample for all 12 immune archetypes. The max score for each sample was identified, and the tumour was then assigned to this immune archetype.

Statistics

All statistical analysis and visualisations were performed in R (v3.6.2). All correlation analysis was performed using the Pearson correlation coefficient. The Shapiro–Wilk test was performed to test for normal distribution, *F*-test for equal variances and the Wilcoxon rank-sum test was used when normally distributed or equal variances were not observed when determining if chemotherapy, radiation or steroid treatment had an effect on T-cell infiltration. Fisher's exact test was performed to assess the statistical association between IHC classification and IPASS immune designation of either T-cell infiltrated or cold.

Results

Deconvolution algorithms poorly distinguish individual cell types in high-risk paediatric solid tumours

The ZERO Childhood Cancer Program sequences high-risk paediatric cancers (< 30% chance of survival) to identify potential molecularly targeted treatments [1]. The ZERO cohort includes diverse cancer subtypes at various treatment stages—diagnosis, refractory, relapsed or secondary disease (Additional file 1: Fig. S2). We assigned tumours first into broad disease groups: tumours of the central nervous system (CNS) ($N = 143$), extracranial solid tumours ($N = 148$) or haematological malignancies (HM) ($N = 56$). We further subdivided tumours into these broad categories by tumour subtype (Additional file 1: Fig. S2). RNA-seq and WGS were performed on 347 samples.

Deconvolution algorithms utilise the expression of key marker genes in bulk RNA-seq data to estimate the relative proportions and types of immune cells present in a sample. We applied CSX, quanTIseq and MCP-counter deconvolution algorithms to identify which tumours might have higher proportions of leucocytes, in particular $CD8^+$ T-cells. Estimations of CD8 T-cell abundance were comparable between algorithms (Additional file 1: Fig. S3a-c), so we subsequently focused on CSX. Unsurprisingly, predictions in haematological malignancies were consistent with the malignancy subtype—myeloid cells predominating in acute myeloid leukaemia, B-cells in B-acute lymphoblastic leukaemia and T-cells in T-cell leukaemia (Fig. 1a, b). All CNS samples had low total immune cell numbers (median = 2.6 cells; range 1.2–7.1). Five extracranial tumours had relatively higher immune cell abundance (> 10) than other samples (median = 2.7; range 1.1–30.6; Fig. 1a). The predominant immune cell type in solid tumours (CNS and extracranial) was M2 macrophages with lymphocytes making up less than 30%, on average, of the total immune cell populations (Additional file 1: Fig. S3d-e). However, there were notable exceptions. Twenty-five per cent of neuroblastoma (NBL) had predominant monocyte populations, as did some Ewing sarcomas (EWS), Wilm's tumours (WT) and medulloblastomas (MB). A malignant peripheral nervous sheath tumour (MPNST), a NBL and an ameloblastic fibrosarcoma (classified as 'sarcoma other') all had activated mast cells comprising greater than 60% of the total immune cell population (Additional file 1: Fig. S3d-e). In 96% of CNS tumours, $CD8^+$ T-cells made up less than 10% (median = 5%; range 0–25%) of the predicted immune infiltrating cells (Fig. 1c). More extracranial tumours had $CD8^+$ T-cells, with 24% of samples having at least 10% (median = 5%; range 0–32%) of the immune infiltrating cells predicted to be $CD8^+$ T-cells (Fig. 1d). Thus, RNA-seq deconvolution of the immune landscape indicates that T-cell infiltrated paediatric tumours are rare.

(See figure on next page.)

Fig. 1 Deconvolution of bulk RNA sequencing in paediatric cancer. **a** Absolute immune cell abundance by CIBERSORTx (CSX) for each patient separated into central nervous system (CNS), extracranial, and haematological malignancies (HM), ordered from the highest number of leucocytes to the lowest. **b** Proportion of all leucocytes (*y*-axis) for each HM patient (*x*-axis) separated into acute myeloid leukaemia (AML), B-precursor acute lymphoblastic leukaemia (BALL) and T-cell acute lymphoblastic leukaemia (TALL). **c**, **d** Proportion of CD8 T-cells in CSX within each patient classed by CNS (**c**) and extracranial (**d**) tumour subtypes

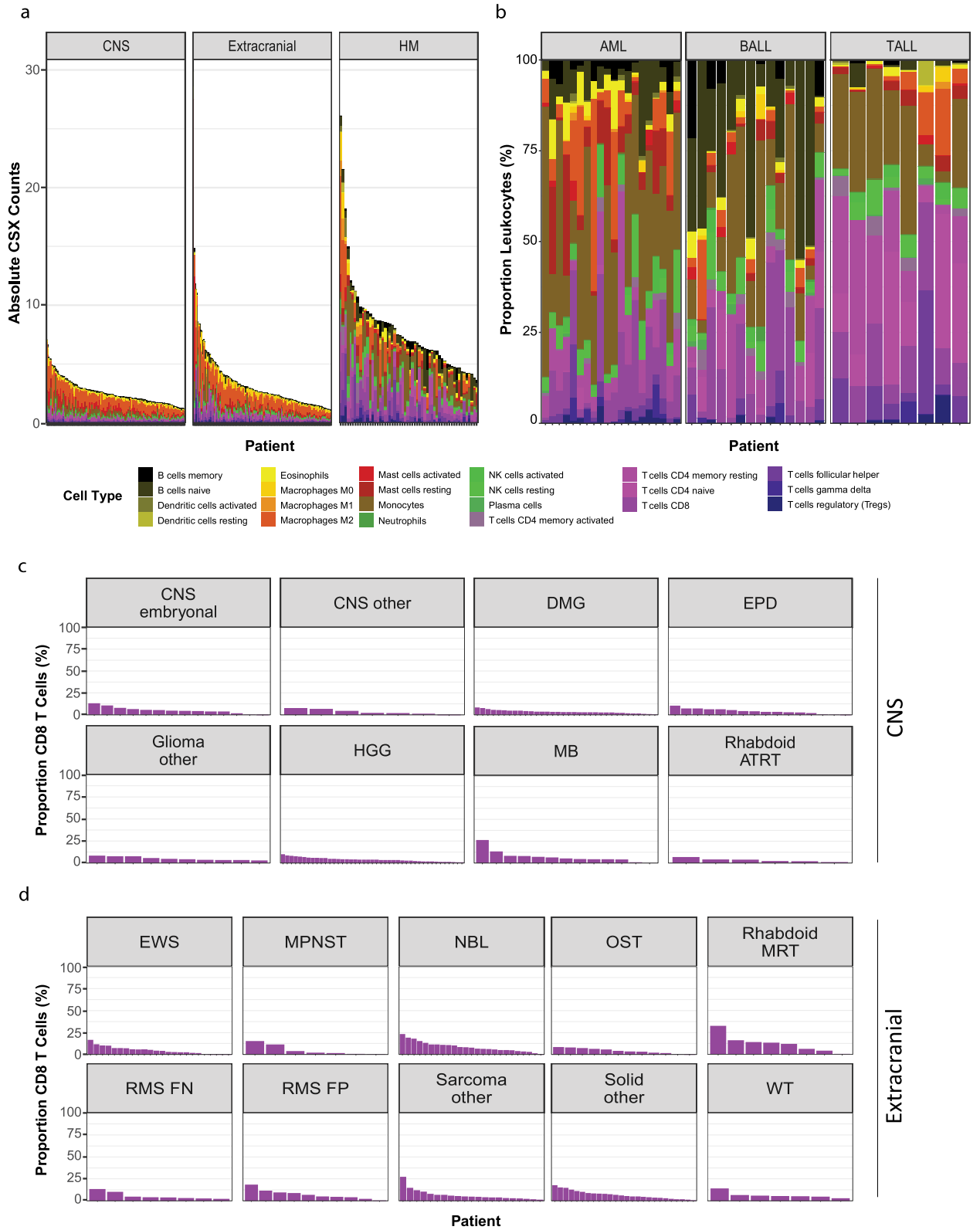

Fig. 1 (See legend on previous page.)

High-risk paediatric cancers are predominantly negative for PD-L1 protein expression

We next explored the relationship between PD-L1 transcript abundance and PD-L1 protein expression in a subset of 59 tumours (20% of the cohort) in which we could perform PD-L1 immunohistochemistry. These included both CNS and extracranial tumours. The samples were independently reviewed by an experienced pathology team, blinded to RNA-seq data, and classified as either PD-L1$^+$ ($\geq$ 1% cells) or PD-L1$^-$ (< 1% cells) using standard clinical criteria [31] (Fig. 2a). Only three samples were definitively PD-L1$^+$ by IHC, one of which had extremely low levels of PD-L1 mRNA (0.69 TPM; Fig. 2b, c). Of the nine tumours with PD-L1 mRNA expression > 3 TPM, only two were PD-L1$^+$ by IHC (Fig. 2c). This suggests that mRNA-based thresholds for identifying PD-L1$^+$ paediatric tumours may not reliably identify tumours which are PD-L1$^+$ by IHC criteria, and PD-L1 TPM-based criteria in clinical trials of checkpoint inhibition require further validation.

Immunohistochemistry identifies immune hot and altered paediatric tumours

We next investigated tumour infiltration by CD45$^+$ cells, CD8$^+$ T-cells and CD4$^+$ T-cells using RNA-seq deconvolution, and independent analysis of IHC staining for these markers. Seventy-eight samples, representing 27% of the cohort, were analysed (Fig. 3a, Additional file 1: Fig. S4a-c). We used image analysis to quantitate the number of positive staining cells per mm^2 (Fig. 3b). In addition, each sample was independently reviewed by a pathologist for CD8$^+$ and CD4$^+$ infiltration, blinded to the computational or image analysis results. Tumours were classified as either immune inflamed ('hot'), non-inflamed ('cold') or immune-excluded ('altered') using published criteria [15] (Fig. 3c). One sample, without an adjacent

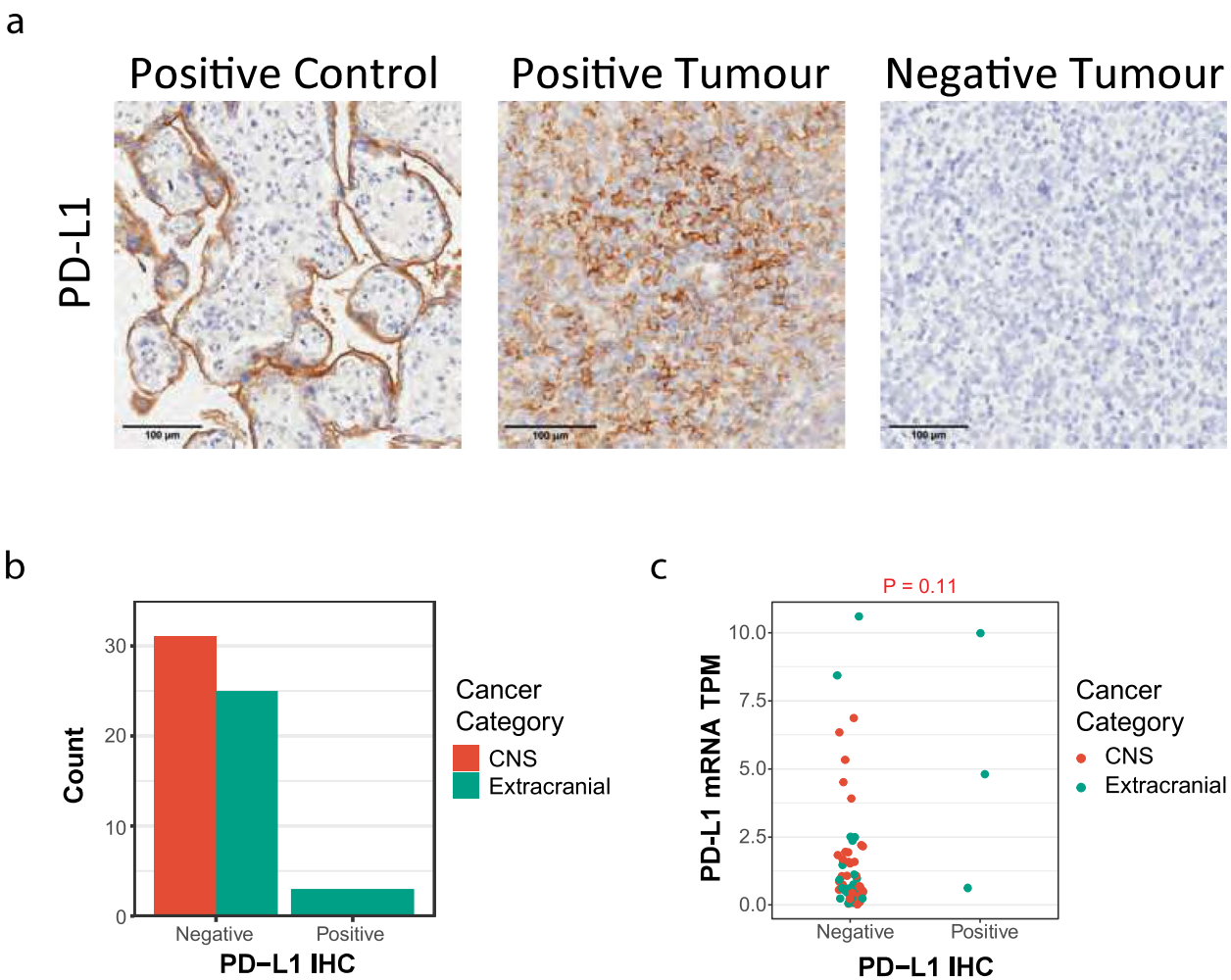

Fig. 2 High-risk paediatric cancers are predominantly PD-L1 negative. **a** Representative immunohistochemistry (IHC) images for PD-L1 in a control, positive and negative tumour. **b** Number of PD-L1-negative and PD-L1-positive samples with cancer category highlighted. **c** PD-L1$^-$ (< 1%) and PD-L1.$^+$ ($\geq$ 1%) by IHC compared to PD-L1 expression by RNA-seq (TPM, transcripts per million) in CNS (red) and extracranial tumours (blue)

haematoxylin and eosin section, was classified as indeterminate. Seventy-six per cent (29/38) of CNS tumours were classified as cold, none as hot and 24% (9/38) were altered. Fewer extracranial tumours were cold (23/39, 59%), 14 were altered (36%) and two hot (5%). Thus, 41% classified as either altered or hot (Fig. 3c). We observed a weak positive correlation between the IHC estimates of total leucocytes to the absolute immune cell abundance predicted by CSX ($P=0.01$, $r=0.26$; Fig. 3d). However, there was no significant correlation between the computational and pathological estimates of the number of $CD8^+$ T-cells ($P=0.15$, $r=0.16$) or $CD4^+$ T-cells ($P=0.8$, $r=0.03$; Fig. 3e, f). This suggested that CSX is not sufficiently sensitive to distinguish individual immune cell types in paediatric samples characterised by low numbers of infiltrating immune cells. The poor correlation between histological and computational predictions of $CD8^+$ T-cell abundance was also true of quanTIseq and MCP-counter (Additional file 1: Fig. S4d-e). The CSX estimate of $CD8^+$ T-cell abundance in the two hot samples was the highest estimate in the extracranial cohort, whereas the estimated $CD8^+$ T-cell abundance in altered and cold samples was similar (Additional file 1: Fig. S4f). Contrasting these data with the accurate leucocyte subtype predictions in haematological malignancies (Fig. 1b) suggests that the computational prediction of the immune microenvironment using the tested algorithms depends on immune cell abundance, which in most paediatric tumours are too low to be reliable.

Corticosteroids, chemotherapy and radiation therapy have the potential to alter the TIME [42]. To explore this, we looked for correlations between these therapeutic interventions and the number of immune cells per mm^2 in tumours. No significant difference was observed for $CD45^+$, $CD8^+$ or $CD4^+$ cells in patients who had received chemotherapy or radiation treatment within 42 days of biopsy in IHC data (Additional file 1: Fig. S5a-c). Furthermore, there was no significant association between corticosteroid administration within 7 days of biopsy and lymphocyte numbers in CNS tumour patients, the population most likely to have received this treatment (Additional file 1: Fig. S5d-f). This indicates that chemotherapy, radiation and corticosteroid administration are unlikely to be confounding variables altering the analysis of the TIME.

A novel immune signature predicts T-cell infiltration in high-risk paediatric tumours

We next used the IHC partitioning of tumours as immune hot, altered or immune cold to define a transcriptional signature to predict $CD8^+$ T-cell infiltration of high-risk paediatric cancers. For this analysis, we clustered immune hot and altered samples together. We applied machine learning (see the 'Methods' section) to generate a 15-gene signature on the training set ($N=34$) which was further applied to the test set ($N=35$) (Fig. 4a). We converted this signature into a score (hereafter referred to as the Immune PAediatric Signature Score (IPASS)) and normalised the IPASS to a range of 1 (most inflamed) to -1 (least inflamed). Using an IPASS of ≥ -0.25 to indicate immune hot/altered and < -0.25 to indicate immune-cold, the IPASS score had a positive predictive value of 78%, a negative predictive value of 92%, a sensitivity of 84% and a specificity of 88%. In the test set, the resultant signature predicted with 87% accuracy the immune classification of the tumours by IHC. This indicates that the IPASS score can independently classify paediatric tumours as immune hot/altered ('T-cell infiltrated') or immune cold.

This gene signature, constructed to identify immune-hot or immune-altered tumours, incorporates immune markers of inflammation and exclusion (Fig. 4a). Increased expression of *NFATC3*, *TNFRSF18 (GITR)*, *NFkb1*, and *CD27* are associated with T-cell activation. NFATC3 is a transcription factor which initiates the production of IL-2 [43], *TNFRSF18* and *CD27* are both T-cell costimulatory molecules [44], NFkb1 is a key transcription factor generated downstream of T-cell receptor (TCR) signalling [45] and CTLA-4 is an immune checkpoint expressed following TCR ligation [46, 47]. Both *CTLA-4* and *TNFRSF18* are highly expressed on Tregs and increased expression re-enforces the Treg suppressor phenotype [44, 48]. *FRP2* (N-formyl peptide receptor 2) is broadly expressed by immune cells and binds several ligands derived from bacterial products leading to initiation of the danger signal response [49], whereas C1 esterase inhibitor is an inflammatory inhibitor [50]. *CXCL9* and *CXCL11* are key chemokines for the trafficking of effector T cells into the tumour and are secreted by macrophages and stromal cells in response to IFN-γ secreted by T-cells [51]. Finally, increased expression of

(See figure on next page.)

Fig. 3 Immunohistochemistry identifies immune-hot and immune-altered paediatric tumours. **a** Representative IHC images for CD45, CD8 and CD4 staining in CNS and extracranial tumours illustrating positive and negative tumours. **b** The number (cells/mm^2) of $CD45^+$, $CD8^+$, and $CD4^+$ cells in CNS and extracranial tumours by IHC. Black horizontal line represents the mean. **c** Number of CNS and extracranial samples classified by CD8 IHC as either immune-cold, immune-altered or immune-hot. **d** Correlation between the absolute number of immune cells by CIBERSORTx (CSX) compared to number/mm^2 of $CD45^+$ cells by IHC. **e** Correlation between the absolute number of CD8 T-cells by CSX compared to number/mm^2 of $CD8^+$ T-cells by IHC. **f** Correlation between the absolute number of CD4 T-cells by CSX compared to number/mm^2 of $CD4^+$ cells by IHC. Blue line in (**d–f**) is the correlation line of best fit

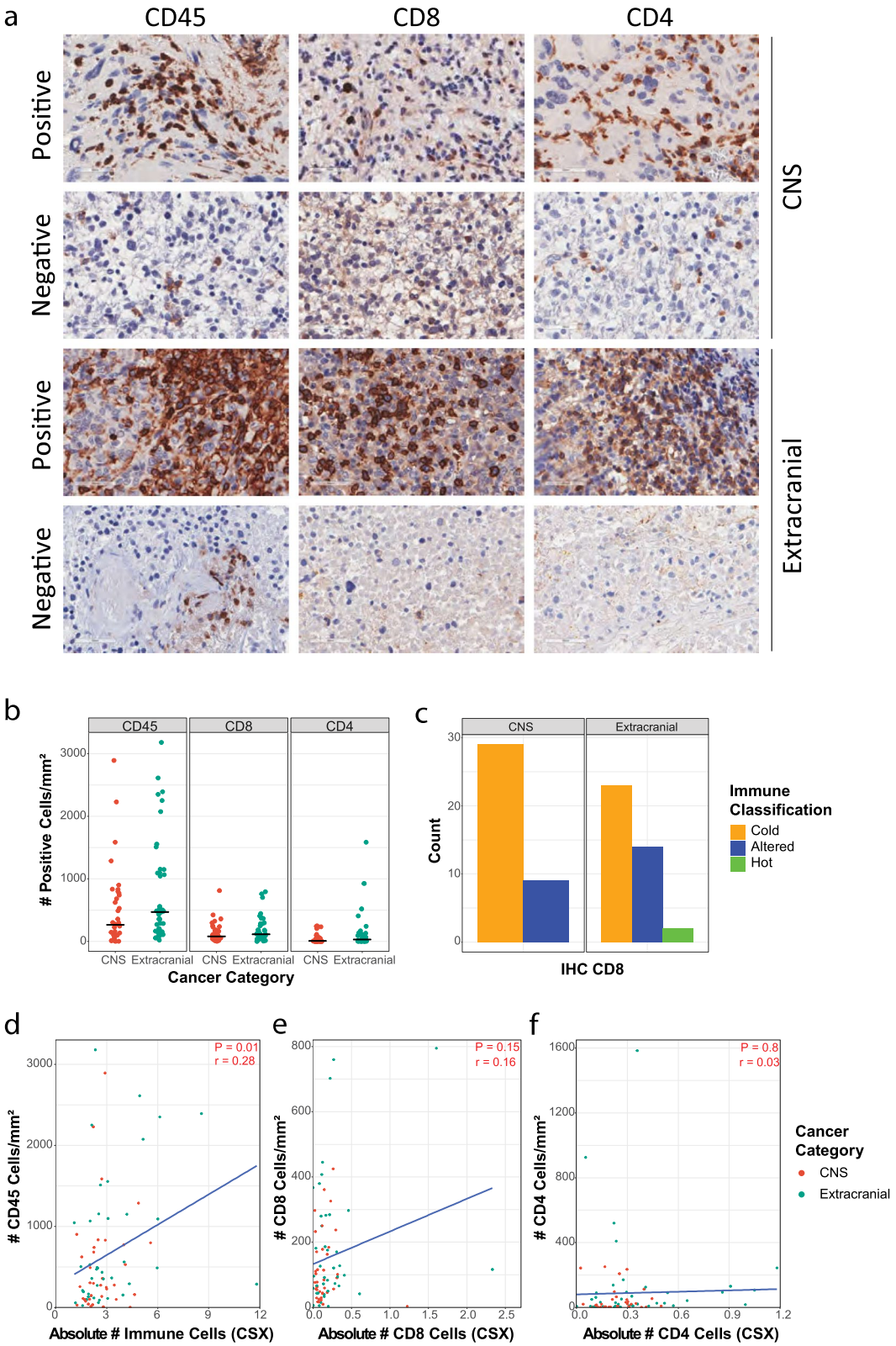

Fig. 3 (See legend on previous page.)

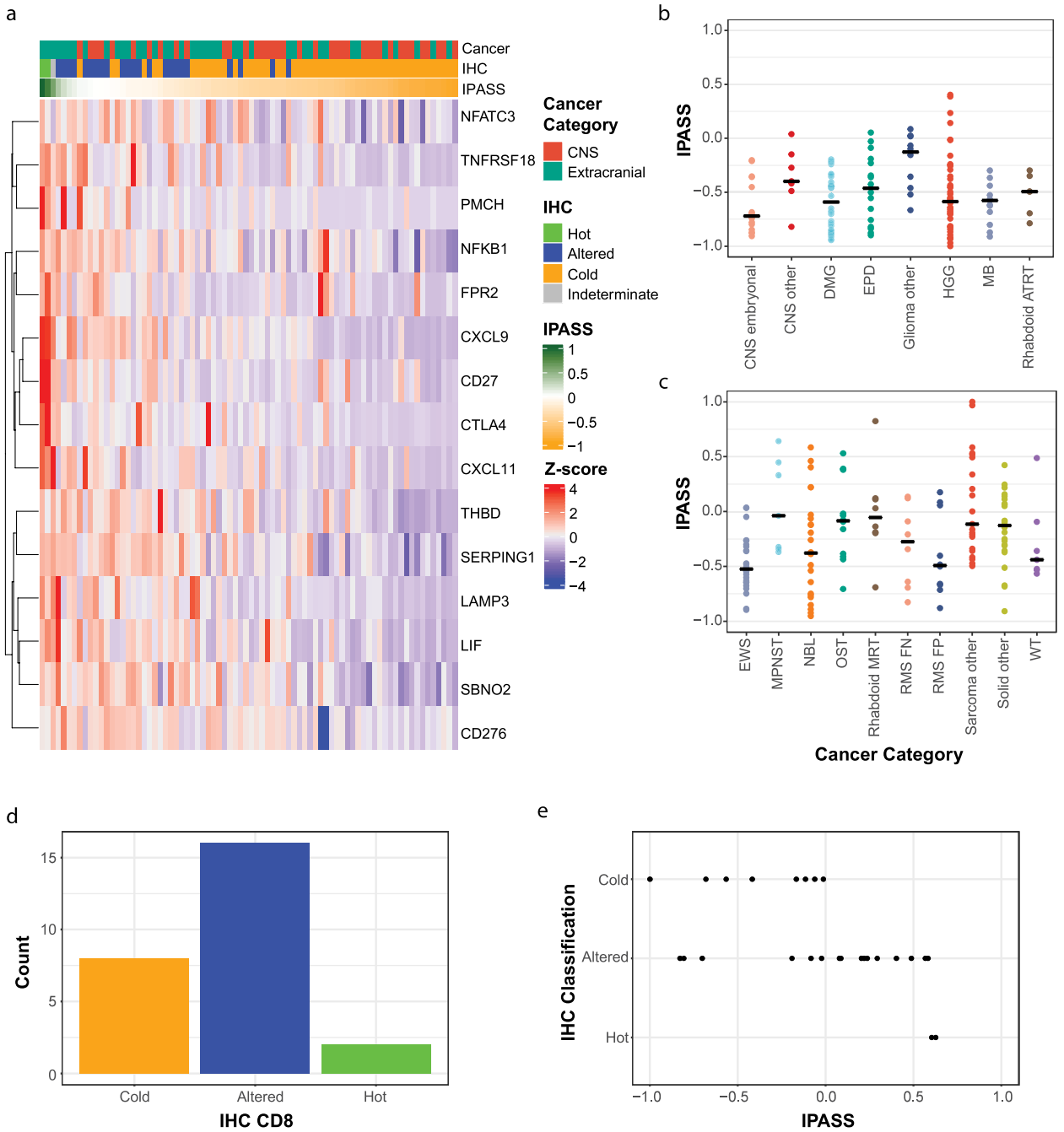

Fig. 4 Novel paediatric immune signature predicts T-cell infiltrated tumours. **a** Heatmap of the novel 15-gene paediatric immune signature (IPASS) in patients with matched IHC ($n = 78$). The top annotation bar represents the cancer category, the second annotation is CD8 IHC classification and the third annotation bar is the normalised IPASS score measured between 1 (green) and − 1 (orange). IPASS distribution across **b** CNS and **c** extracranial tumours. **d** Number of validation samples classified by CD8 IHC as either immune-cold, immune-altered or immune-hot. **e** IPASS for each validation sample assigned to their IHC CD8 classification ($n = 26$)

LAMP3 (DC-LAMP) and *CD141* (THBD or *BDCA-3*) [52] are expressed by mature and cross-presenting dendritic cell subsets. The transcriptional repressor *SBNO2* is expressed in macrophages following IL-10/STAT3 signalling and contributes to the anti-inflammatory response [53]. Finally, *B7-H3* expression by tumour cells is immune suppressive and a current target for immunotherapy strategies [54].

We applied the IPASS to the remaining samples ($n=213$) in our cohort. From all 291 samples, 102 T-cell infiltrated CNS and extracranial solid tumours were predicted (Fig. 4b, c, Additional file 1: Fig. S6a-b). Twenty per cent (29/143) of CNS tumours had T-cell infiltrated IPASS compared to 49% (73/148) of extracranial tumours (Fig. 4b, c, Additional file 1: Fig. S6a-b). This is in concordance with the proportions identified by the IHC classification (Fig. 3c). T-cell infiltrated tumours were identified across all tumour subtypes except atypical teratoid rhabdoid tumours (ATRT) (Fig. 4b, c). In addition, 21% of high-grade gliomas (HGG) and 15% of diffuse midline glioma (DMG), tumour subtypes sometimes considered non-inflamed [55, 56], had IPASS scores predicting T-cell infiltration (Fig. 4b, Additional file 1: Fig. S6a). Of the extracranial tumours, relapsed neuroblastoma and MPNST had the highest proportion of immune-infiltrated tumours. Individual examples of epithelioid sarcoma and alveolar soft part sarcoma (both sub-classed as 'sarcoma other') had the highest IPASS (Fig. 4c, Additional file 1: Fig. S6b). In keeping with our IHC results (Additional file 1: Fig. S5), IPASS was unaffected by prior treatment or corticosteroid administration (Additional file 1: Fig. S6a-b).

We tested the validity of the IPASS in an independent dataset (see 'Methods' section) which underwent bulk RNA-seq and IHC analysis as described for the original cohort. IHC classification in the validation dataset identified 8 cold, 16 altered and 2 hot tumours, which were significantly associated with the IPASS (Fisher's exact $p=0.01$; Fig. 4d, e). Extending the IPASS to all samples within the independent dataset that had RNA-seq ($N=121$) identified twenty-six T-cell infiltrated tumours in an independent dataset (Additional file 1: Fig. S6c). Taken together, applying the IPASS to ZERO and the validation cohorts suggests that 31% (128/412) of childhood solid tumours are T-cell infiltrated, with the majority falling into the 'altered' category, and up to 4% may be true 'hot' tumours (Additional file 1: Fig. S6a-c).

IPASS correlates with other markers of immune infiltration

T-cell receptor (TCR) clonal diversity within a tumour has been linked to adaptive immune responses as it increased the capacity for T-cells to recognise antigens [57]. For extracranial solid tumours and CNS tumours, we calculated the number of T-cell clones present in each sample from bulk RNA-seq data and tested the correlations with IPASS (Additional file 1: Fig. S6d-e). The 'glioma other' subgroup (anaplastic pleomorphic xanthoastrocytoma, ganglioglioma and progressive low-grade glioma) had the highest number of TCR clones of the CNS tumours. Osteosarcoma and neuroblastoma had the highest TCR diversity of the extracranial tumours. The number of T-cell clones positively correlated with IPASS ($P=1.2e-11$, $r=0.39$; Fig. 5a, Additional file 1: Fig. S6f).

Elevated tumour-specific neoantigen load is associated with an increased presence of T-cells, particularly in the context of adult tumours with high mutation burdens or childhood cancers arising as a result of germline mutations in mismatch repair genes [25]. This relationship is far less clear in paediatric cancers with much lower mutation burdens. We explored the relationship between the IPASS, TMB and neoantigen burden. There was a wide variation of neoantigen load across tumour types (Additional file 1: Fig. S7a-b). HGG had the greatest range (5–528), and of the 'CNS other' group, 2 choroid plexus carcinomas had over 200 predicted neoantigens (Additional file 1: Fig. S7a). In extracranial tumours, neoantigen load ranged from 1 to 416, with 4 MPNST samples having > 100 predicted neoantigens. High individual neoantigen loads were also observed in adrenocortical carcinoma and malignant germ cell tumour (both sub-classed as 'solid other') (Additional file 1: Fig. S7b). As anticipated, a significant correlation was observed between the number of neoantigens and the TMB ($P=2.2e-16$, $r=0.57$; Additional file 1: Fig. S7c). However, neither the TMB nor the number of neoantigens positively correlated with the IPASS ($P=0.86$, $r=-0.01$ and $P=0.96$, $r=0.0$, respectively; Fig. 5a, Additional file 1: Fig. S7d-e). This suggests that the quantity of mutations and neoantigens is not predictive of T-cell tumour infiltration in paediatric cancers which have mutation burdens within the non-hypermutated range (< 5 mut/MB). Interestingly, there was a significant negative correlation between the IPASS score and estimated tumour purity using WGS data ($P=1.6e-14$, $r=-0.43$; Additional file 1: Fig. S7f). This might be expected if the TIME and other non-tumour cells make up a greater proportion of the sequenced sample. Together, these data establish that neoantigen load

(See figure on next page.)

Fig. 5 Immune genes and archetypes provide insight into TIME of paediatric tumours. **a** Heatmap of 12 immune checkpoint genes associated with IPASS in extracranial tumours ($n=148$). The top annotation bar represents the cancer category, the second annotation is CD8 IHC classification and the third annotation bar is the normalised IPASS score measured between 1 (green) and − 1 (orange). Below the heatmap, the annotation bars represent the number of T-cell receptor (TCR) clones, tumour purity (percentage of malignant cells), tumour mutation burden (TMB) and neoantigen load. **b**, **c** IPASS score (highlighted by hot/altered (red) or cold (blue)) for each sample assigned to their given dominant immune archetype in **b** CNS and **c** extracranial tumours. Archetype key: dendritic cells (DC), immune stromal rich (ISR), immune rich (IR), classical DC (cDC) and immune desert (ID)

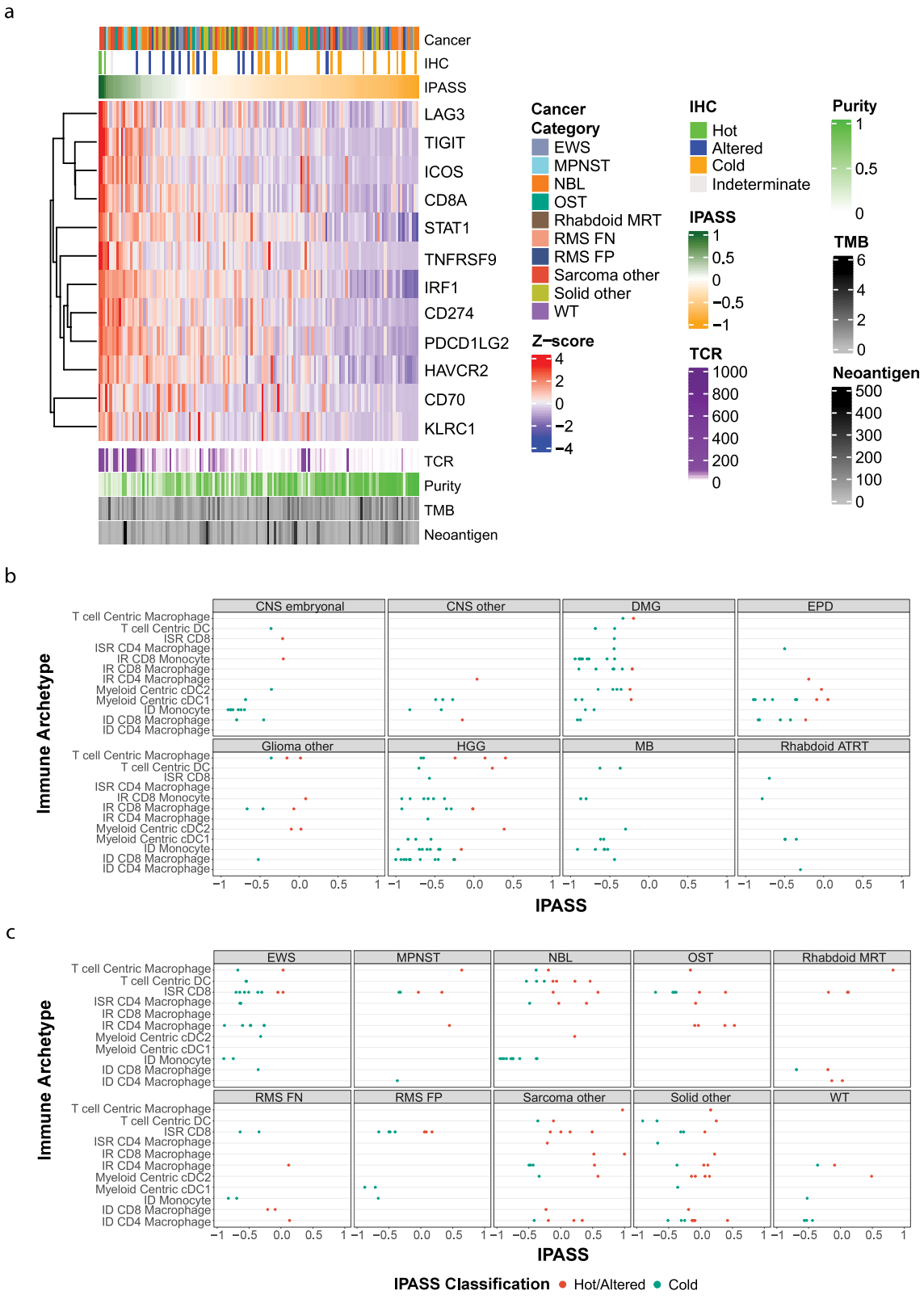

Fig. 5 (See legend on previous page.)

and TMB are not indicative of T-cell infiltrated phenotype in most paediatric solid tumours.

We next characterised the expression of a selected list of immune checkpoint and regulatory genes (Additional file 1: Table S1) to identify those most associated with an IPASS > −0.25, in order to understand the potential immune suppression mechanisms regulating T-cell infiltration in high-risk childhood cancers. A subset of 12 genes showed a strong statistical association with high IPASS scores by *K*-means clustering (Fig. 5a, Additional file 1: Fig. S7g-h). These include members of the TNF-receptor superfamily *CD70* and *TNFRSF9* (CD137, 41BB), Programmed-death ligands 1 and 2 (*CD274* and *PDCD1LG2*), lymphocyte-activation gene 3 (*LAG3*) and T-cell immunoglobulin genes *TIGIT* and *TIM3* (Fig. 5a). Taken together, increased expression of these genes is a further indication that elevated IPASS is indicative of T-cell activation within these tumours. In CNS tumours, these 12 immune genes were weakly associated with higher IPASS scores, in part because fewer CNS samples had scores indicative of T-cell infiltration (Additional file 1: Fig. S7g).

T-cell tumour infiltration may be indicative of several distinct immune archetypes, both immune rich (IR) and immune desert (ID), within the TIME [41]. We used expression signatures associated with immune archetypes to explore the associations between the IPASS and IR and ID immune archetypes (Fig. 5b, c; Additional file 1: Fig. S7i-j). Higher IPASS scores were significantly more likely to be associated with IR archetypes ($P = 0.0026$). Most CNS tumours were ID and dominated by archetypes associated with high numbers of monocytes or macrophages (Fig. 5b). There were more IR archetypes in extracranial tumours but no associations of statistical significance with tumour subtypes, indicating the diverse archetypes across our cohort are not constrained by tumour type. Some trends, such as the predominance of the monocyte archetype in ID neuroblastoma and the lack of any osteosarcomas with an ID archetype of any sort, may prove significant in larger cohorts. However, the association between the higher IPASS scores and IR archetypes indicates that IPASS is identifying immune-infiltrated TIME in most paediatric cancer types. The detailed nature of the TIME appears to vary at an individual level.

Discussion

The tumour transcriptome provides high-resolution insights into the cellular and molecular basis of individual tumours and the surrounding TIME [1, 2]. We set out to characterise the TIME from the sequencing performed in the ZERO Childhood Cancer programme; however, most tools that are used to deconvolute the immune signature from bulk RNA-seq data have been developed from adult cancer data sets [21–23]. Thus, we developed a paediatric cancer-specific transcriptional tool, based on a 'ground truth' of IHC classification of inflammation status (inflamed, excluded or desert) through integrating these findings with RNA-seq. One important motivation is that many current biomarkers used as surrogates for inflamed tumours, such as TMB, neoantigen load and PD-L1 transcript expression [25, 58, 59] have limited applicability in the paediatric setting, where mutation burdens and neoantigen abundance are far lower than in most adult cancers [26]. Thus, whilst we show that neoantigen load correlates with TMB, neither variable correlates with T-cell infiltration. Moreover, if the true HLA affinity threshold is lower than commonly used for neoantigen prediction, then the number of true antigens in paediatric tumours may be even lower than in silico predictions [60]. Therefore, beyond the small subset of paediatric patients with hypermutated tumours, an important challenge is to characterise the TIME of paediatric tumours with more typical TMB (< 5 muts/Mb). Our data clearly indicate that a proportion of such tumours do harbour infiltrating T-cells. The specific tumour epitopes presented to and recognised by infiltrating T-cells may be more critical for potential T-cell responses than the absolute neoantigen load.

An important relationship we explored is that between the PD-L1 gene and protein expression on tumour cells or antigen-presenting cells. The importance of this relationship is emphasised as PD-L1 gene expression is a criterion on which paediatric patients are selected for in a trial of anti-PD-L1 therapy [58]. Appropriate selection of patients is critical to trial success, and our data may provide one explanation for the limited anti-tumour activity to ipilimumab, pembrolizumab, nivolumab and atezolizumab seen in paediatric patients [11, 12, 61, 62]. In our cohort, PD-L1 protein expression cannot be reliably predicted from RNA-seq data. This is in part because the transcript expression is, in most instances of paediatric cancer, very low (median TPM 0.92) and likely below levels where the relationship between transcript abundance becomes a reliable predictor of protein abundance. There is a poor correlation between PD-L1 mRNA expression levels and protein levels in paediatric cancers. Furthermore, data from phase I clinical trials of checkpoint inhibitors in childhood cancers shows that PD-L1 mRNA levels are a weak predictor of clinical response, even whilst most responders are PD-L1 positive by IHC [12, 13]. This suggests that PD-L1 IHC has greater utility than mRNA transcript abundance, but alone is not sufficient to predict response. Low transcript levels of PD-L1 do not necessarily indicate that a tumour lacks PD-L1 protein. Using PD-L1 transcript counts, 15% of our cohort

would be eligible for trial inclusion but only two of these had unequivocal evidence of PD-L1 protein expression. Conversely, the TPM criteria would have excluded a patient who was, by IHC, PD-L1^{+}. The better informed patient selection might improve the generally disappointing results of anti-PD-1 immunotherapies in paediatrics, as is becoming clearer in the use of these agents in hypermutated tumours [25] and INI-negative tumours [63].

The IPASS score is primarily to detect T-cell infiltration of high-risk paediatric cancers. Our data suggests that there are subsets of paediatric tumours, thought previously not to be inflamed, which may in fact harbour a diverse T-cell repertoire. The questions this raises are what antigens are these T-cells responding to and what immunosuppressive pathways characterise individual paediatric cancers? The IPASS gene signature not only identified genes indicative of T-cell activation (from the 'hot' samples) but also genes involved in the suppression of T-cell responses (from the 'altered' samples), across a broad range of childhood cancers. We have represented the IPASS in a conceptual diagram depicting the tumour immune cellular and signalling network (Fig. 6). Thus,

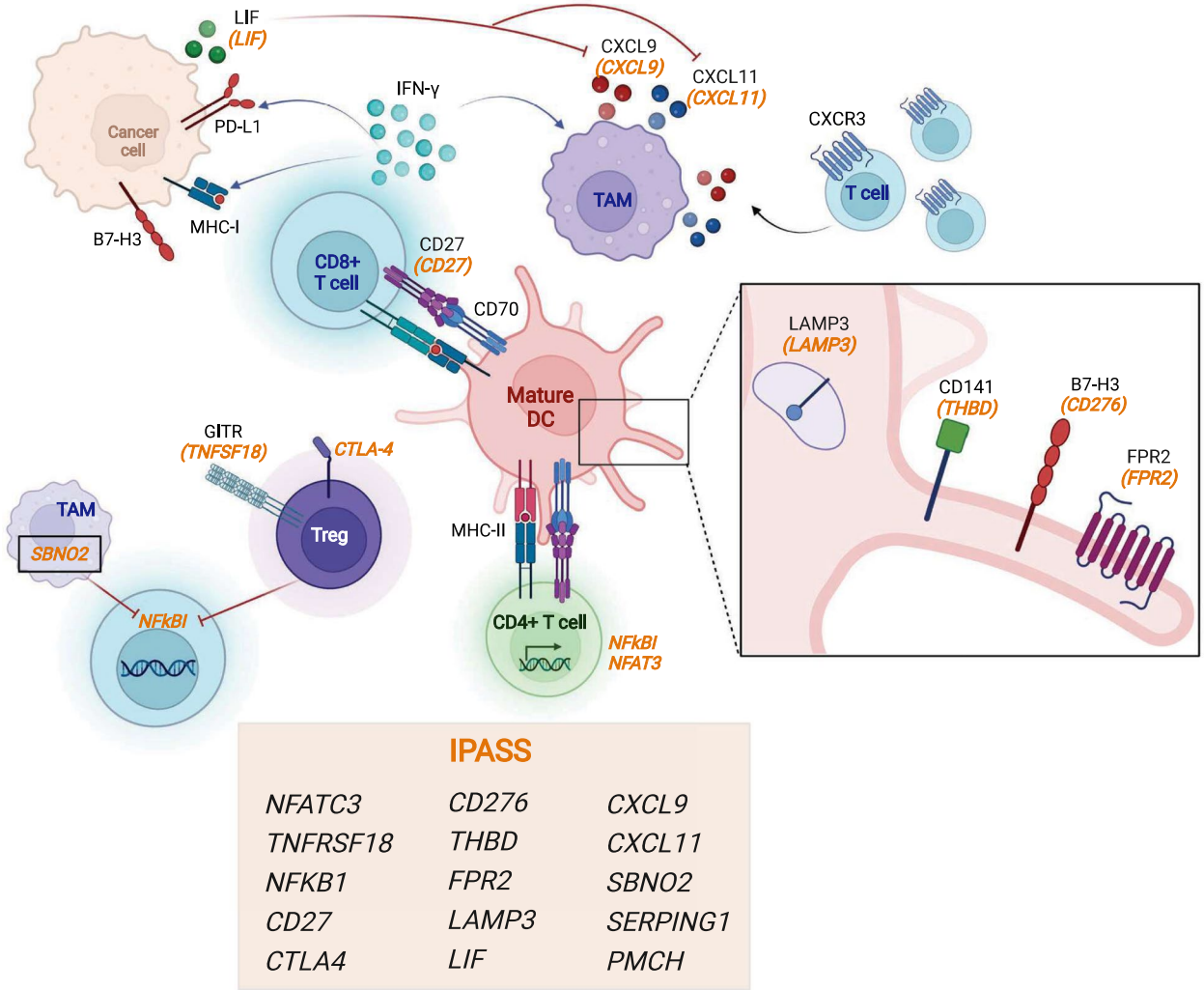

Fig. 6 The IPASS gene signature describes a complex immune network within paediatric cancers. A concept figure depicting the potential immune cell interactions which feature the IPASS genes. The IPASS describes interactions which both drive and control anti-tumour immunity. CD8^{+} T-cells (blue) recognise tumour-associated antigen on mature and cross-presenting dendritic cells (pink) [*CD141*, *LAMP3*] and secrete IFN-γ, which induces cancer cell MHC-I and PD-L1 expression. IFN-γ response genes [*CXCL9*, *CXCL11*] are derived from tumour associated macrophages (TAMs, mauve) and are key chemokines for trafficking of CXCR3^{+} effector T-cells into the tumour. Control over this effector T-cell trafficking is mediated by tumour cell secretion of *LIF* which suppresses TAM *CXCL9*. In addition, IL-10/STAT3 signalling in TAMs induces *SBNO2*, a transcriptional co-repressor which contributes to the anti-inflammatory response. The IPASS includes genes expressed by activated T-cells [*NFATC3*, *NFKb1*, *CD27*, *CTLA4*, *GITR*], in contrast to the immune suppressor Tregs (purple) constitutively express [*GITR*, *CTLA4*]. The functional effect of *B7-H3* is context dependent, *B7-H3* expression on tumour cells is immune suppressive. The transmembrane receptor *FPR2* senses ligands from bacteria products and generates a danger signal. This figure was created in Biorender

whilst increased expression of *NFATC3*, *TNFRSF18*, *NFkb1*, *CD27* and *CTLA4* are indicative of T-cell activation [43–47, 64], *TNFRSF18* and *CTLA4* are also highly expressed on Tregs, which are involved in downregulating antitumour immune responses [44, 48]. CD70 is expressed on antigen-presenting cells and co-stimulates T-cell via binding to CD27 [64]. CD137 [65] is also a costimulatory molecule expressed on activated T-cells within tumours, along with the immune checkpoints LAG3, TIM3 and TIGIT [66]. Whilst PD-L2 is constitutively expressed by antigen-presenting cells [67], PD-L1 is upregulated on tumour cells and antigen-presenting cells following IFN-γ stimulation [68]. The expression of leukaemia inhibitory factor (*LIF*) is a novel feature of the IPASS, as LIF has not previously been identified as a prominent feature of the TIME in paediatric cancer. LIF is a ligand for the LIF receptor (LIFR) and a member of the interleukin-6 cytokine family [69]. LIF has immunosuppressive functions in some tumour contexts, in part by repressing CXCL9 (also part of the IPASS) and $CD8^+$ T-cell infiltration of tumours [70]. Establishing the role of LIF in the TIME of childhood cancers potentially opens up the possibility of combined LIF inhibition and anti-PD-L1 immunotherapy.

A pan-cancer score like IPASS is necessarily reductive, focused on developing validated and robust ways of characterising immune-altered and hot tumours across the broad spectrum of paediatric oncology pathologies, but sacrificing some of the detailed individual features of the TIME. Furthermore, the numbers of samples across all tumour subtypes on which we have IHC also limit the resolution of the score. We tried to address this by exploiting other expression-based signatures developed following high-resolution characterisations of the cell type and gene-expression profiles of a broad, adult pan-cancer cohort [41]. This showed, at one level, that our IPASS score is identifying samples with immune-rich signatures, and with a bias towards T-cell infiltration. Furthermore, there are also diverse TIMEs both within tumour subtypes and across the paediatric pan-cancer landscape. Although the numbers of tumours in each subtype limited the capacity to establish definitive links between tumour types and TIME archetypes, it is likely that such patterns will emerge with expanded sequencing of paediatric tumours, particularly if the presentation of certain tumour-specific antigens, for example, fusion oncogenes, are important in invoking a T-cell response.

Conclusions

Combining the IPASS with other approaches such as the immune archetypes provides a more nuanced and detailed insight into the specific mechanisms operating within individual cancers that distinguish hot and altered tumours from cold tumours, and the complex mechanism of immune evasion. This, we propose, will be the basis of detailed understanding of the immunological features unique to paediatric cancers, and the development of therapeutic approaches that can realise the potential of immunotherapy in solid childhood cancers. A key question to be tested in future clinical trials is whether a score such as IPASS identifies a population of high-risk childhood cancers with an inflamed tumour microenvironment that are more likely to benefit from immunotherapies. By bringing together molecular and clinical response data across multiple clinical trials, it may be possible to refine biomarkers of clinical response.

Abbreviations

ATRT	Atypical teratoid rhabdoid tumours
CNS	Central nervous system
CTLA-4	Cytotoxic T lymphocyte antigen 4
CSX	CIBERSORTx
DMG	Diffuse midline glioma
EWS	Ewing sarcomas
HGG	High-grade gliomas
HM	Haematological malignancies
ID	Immune desert
IHC	Immunohistochemistry
IPASS	Immune PAediatric Signature Score
IR	Immune rich
MB	Medulloblastomas
MPNST	Malignant peripheral nervous sheath tumour
NBL	Neuroblastoma
NCH	Nationwide Children's Hospital
PD1	Programmed cell death 1
PD-L1	PD1 ligand 1
RNA-seq	RNA sequencing
TCR	T-cell receptor
TIL	Tumour infiltrating leucocytes
TIME	Tumour immune microenvironment
TMB	Tumour mutation burden
TPM	Transcripts per million
WGS	Whole-genome sequencing
WT	Wilm's tumours

Supplementary Information

The online version contains supplementary material available at https://doi.org/10.1186/s13073-023-01170-x.

Additional file 1: Table S1. Immune checkpoint and regulatory genes. **Fig. S1.** PRISM clinical trial study schema. **Fig. S2.** Cohort overview. **Fig. S3.** Deconvolution algorithms exhibit high concordance and an abundance of M2 macrophages in paediatric cancer. **Fig. S4.** Immunohistochemistry identifies paediatric patients with T-cell infiltrated tumours. **Fig. S5.** Prior treatment and steroid administration do not significantly affect T-cell infiltration. **Fig. S6.** Distribution of IPASS and T-cell clones are heterogenous across histologies. **Fig. S7.** IPASS correlations with additional markers of immune infiltration.

Acknowledgements

We sincerely thank patients and parents for participating in this study. We thank the many clinicians, tumour banks and health professionals for their time acquiring consent for patients and for the collection and coordination of samples and associated clinical data at Sydney Children's Hospital, Randwick; the Children's Hospital at Westmead; the John Hunter Children's Hospital; the Queensland Children's Hospital; the Royal Children's Hospital Melbourne; the

Monash Children's Hospital; the Adelaide Women & Children's Hospital; and the Perth Children's Hospital. Tumour samples and coded data were supplied by the Children's Cancer Centre Biobank at the Murdoch Children's Research Institute and The Royal Children's Hospital (mcri.edu.au/research/projects/childrens-cancer-centre-biobank). The establishment and running of the Children's Cancer Centre are made possible through generous support by Cancer In Kids @ RCH (www.cika.org.au), the Royal Children's Hospital Foundation and the Murdoch Children's Research Institute. We thank ANZCHOG as the trial sponsor, and we thank the staff of the Personalised Medicine Theme of the Children's Cancer Institute for their dedicated work on the Zero Childhood Cancer Program. We thank the Biomedical Imaging Facility (BMIF) at UNSW for the access to instruments through which the imaging component of the IHC analysis for this study was carried out. Zero Childhood Cancer is a joint initiative led by the Children's Cancer Institute and the Kids Cancer Centre, Sydney Children's Hospital, Randwick. K.E.M., C.E.C. and E.R.M. wish to thank the Nationwide Foundation Pediatric Innovation Fund (Columbus, OH, USA). The authors would like to acknowledge Luminesce Alliance—Innovation for Children's Health for its contribution and support. Luminesce Alliance—Innovation for Children's Health is a not-for-profit cooperative joint venture between the Sydney Children's Hospitals Network, the Children's Medical Research Institute and the Children's Cancer Institute. It has been established with the support of the NSW Government to coordinate and integrate paediatric research. Luminesce Alliance is also affiliated with the University of Sydney and the University of New South Wales Sydney.

Authors' contributions

V.T. and E.V.A.M. led and managed the Zero Childhood Cancer Program. M.H. and G.M.M conceived and designed the Zero Childhood Cancer Project. R.T., V.Q., D.M, D.S.Z, O.V., P.G.E., J.A.T. and P.J.N provided expertise in cellular immunology and immunotherapy. C.M., M.W., R.B.J. and M.J.C. developed and performed the bioinformatic methods pertaining to WGS. C.M. developed the bioinformatic methods pertaining to RNA-seq and performed computational analysis and integration of the data. F.A., H.T., L.D.P., A.S.M., W.N., N.G.G., G.M., J.R.H., S.L.K., P.J.W., T.N.T., G.M.M. and D.S.Z were clinical leads at the recruiting centres and coordinated the patient selection. L.M.S.L., D.K., M.K.M., D.G., A.S., N.Z., N.O., H.D., F.A., H.T. and Y.D. collected the patient treatment information. K.E.M., C.E.C. and E.R.M. provided additional RNA and patient slides for the external validation cohort. A.J.G. provides pathology expertise. A.J.G., F.S. and T.S. analysed IHC data. R.T. and P.R. optimised and stained for CD45, CD4 and CD8. A.Y. and D.C. optimised and stained for PD-L1. C.M., M.J.C., J.A.T., P.J.N. and P.G.E. conceived, designed and wrote the manuscript with comments and contributions from all authors. The authors read and approved the final manuscript.

Funding

This work has been funded by the Australian Federal Government Department of Health, the New South Wales State Government and the Australian Cancer Research Foundation for funding to establish infrastructure to support the Zero Childhood Cancer personalised medicine programme. Funding from the Kids Cancer Alliance, Cancer Therapeutics Cooperative Research Centre supports the development of a personalised medicine programme; Tour de Cure supports tumour biobank personnel; the Steven Walter Children's Cancer Foundation and the Hyundai Help 4 Kids Foundation support G.M.M. and P.G.E.; Samuel Nissen Charitable Foundation supports P.G.E.; the Lions Kids Cancer Genome Project is a joint initiative of Lions International Foundation, the Australian Lions Children's Cancer Research Foundation (ALCCRF), the Garvan Institute of Medical Research, the Children's Cancer Institute and the Kids Cancer Centre, Sydney Children's Hospital. Lions International and ALCCRF provided funding to perform WGS and for key personnel, with thanks to J. Collins for project governance and advocacy. The Cure Brain Cancer Foundation supports the RNA sequencing of patients with brain tumours; the Kids Cancer Project supports molecular profiling and molecular and clinical trial personnel; and the University of New South Wales, W. Peters and the Australian Genomics Health Alliance provide personnel funding support. The Medical Research Future Fund, Australian Brain Cancer Mission/National Health & Medical Research Council/Lifting Clinical Trials and Registry Capacity (NHMRC MRF9500002), the Minderoo Foundation's Collaborate Against Cancer Initiative and funds raised through the Zero Childhood Cancer Capacity Campaign, a joint initiative of Children's Cancer Institute and the Sydney Children's Hospital Foundation, supported the national clinical trial and associated clinical and research personnel. Cancer Institute of New South Wales and New South Wales Health (fellowship funding for M.J.C.; CINSW Early Career Fellowship 181430 for M.K.M; CINSW Program Grant 2019/TPG2037). National Health and Medical Research Council (career development fellowship APP1164960 for O.V.). This research was supported by an Australian Government Research Training Program (RTP) Scholarship (for C.M.). This research was supported by Tour de Cure and the Australia and New Zealand Sarcoma Association (funding for R.T.). The 2018 Priority-Driven Collaborative Cancer Research Scheme, co-funded by Cancer Australia and My Room, for personnel and computational support (grant no. 1165556 awarded to M.J.C.).

Availability of data and materials

Raw RNA sequencing data generated by this study are available from the European Genome-phenome Archive under accession number EGAS00001004572 (https://ega-archive.org/studies/EGAS00001004572) [71] and EGAS00001007029 (https://ega-archive.org/studies/EGAS00001007029) [72]. Scripts related to this publication are available at https://github.com/CCICB/iPASS/ [73].

Declarations

Ethics approval and consent to participate

Each patient provided written informed consent as part of the Australian ZERO Childhood Cancer Precision Medicine programme upon enrolment into either the TARGET pilot programme or the PRISM clinical trial. Ethics for TARGET was approved by the Sydney Children's Hospitals Network Human Research Ethics Committee (LNR/14/SCH/497). Ethics for PRISM was approved by the Hunter New England Human Research Ethics Committee of the Hunter New England Local Health District (reference no. 17/02/015/4.06) and the New South Wales Human Research Ethics Committee (reference no. HREC/17/HNE/29). The research conformed to the principles of the Helsinki Declaration.

Consent for publication

Not applicable.

Competing interests

P.G.E receives an annual payment related to the Walter and Eliza Hall Institute distribution of royalties scheme. P.G.E. consults for Illumina. P.J.N. receives research funding from BMS, Roche Genentech, Allergan, Compugen, Merck Sharpe Dohme and Crispr therapeutics. J.R.H. declares honorarium or Bayer and Alexion Pharmaceuticals; Boxer Capital unrelated to this work. The remaining authors declare that they have no competing interests.

Author details

[1]Children's Cancer Institute, Lowy Cancer Research Centre, UNSW, Kensington, NSW, Australia. [2]School of Clinical Medicine, UNSW Medicine & Health, UNSW Sydney, Kensington, NSW, Australia. [3]University of New South Wales Centre for Childhood Cancer Research, UNSW, Kensington, NSW, Australia. [4]Anatomical Pathology, NSW Health Pathology, Prince of Wales Hospital, Randwick, NSW, Australia. [5]Kids Cancer Centre, Sydney Children's Hospital, Randwick, NSW, Australia. [6]Children's Cancer Centre, Royal Children's Hospital, Parkville, VIC, Australia. [7]Murdoch Children's Research Institute, Royal Children's Hospital, Parkville, VIC, Australia. [8]Cancer Immunology Program, Peter MacCallum Cancer Centre, Parkville, VIC, Australia. [9]The Sir Peter MacCallum Department of Oncology, University of Melbourne, Parkville, VIC, Australia. [10]The Steve and Cindy Rasmussen Institute for Genomic Medicine, Nationwide Children's Hospital, Columbus, OH, USA. [11]Department of Pediatrics, The Ohio State University College of Medicine, Columbus, OH, USA. [12]Tumour Bank, Children's Hospital Westmead, Westmead, NSW, Australia. [13]School of Computer Science and Engineering, UNSW Sydney, Kensington, NSW, Australia. [14]School of Biomedical Engineering, UNSW Sydney, Kensington, NSW, Australia. [15]Cancer Centre for Children, Children's Hospital Westmead, Westmead, NSW, Australia. [16]Monash Children's Hospital, Melbourne, VIC, Australia. [17]Centre for Cancer Research, Hudson Institute of Medical Research, Clayton, VIC, Australia. [18]Department of Paediatrics, School of Clinical Sciences at Monash Health, Monash University, Clayton, VIC, Australia. [19]Oncology Service, Children's Health Queensland Hospital & Health Service, Brisbane, QLD, Australia. [20]The University of Queensland Frazer Institute, Faculty of Medicine, The University of Queensland, Brisbane, QLD, Australia. [21]Department of Paediatric and Adolescent Oncology and Haematology, Perth Children's Hospital, Nedlands, WA, Australia. [22]Brain Tumour Research Program, Telethon Kids Institute, Nedlands,

WA, Australia. [23]John Hunter Children's Hospital, New Lambton Heights, NSW, Australia. [24]Michael Rice Cancer Centre, Women's and Children's Hospital, South Australia Health and Medical Research Institute, Adelaide, SA, Australia. [25]Child Health Research Centre, The University of Queensland, Brisbane, QLD, Australia. [26]School of Medicine, The University of Queensland, Brisbane, QLD, Australia. [27]South Australia ImmunoGENomics Cancer Institute, University of Adelaide, Adelaide, SA, Australia. [28]Department of Pathology, The Ohio State University College of Medicine, Columbus, OH, USA. [29]Department of Neurosurgery, The Ohio State University College of Medicine, Columbus, OH, USA.

Received: 13 October 2022 Accepted: 8 March 2023
Published online: 03 April 2023

References

1. Wong M, Mayoh C, Lau LMS, Khuong-Quang DA, Pinese M, Kumar A, et al. Whole genome, transcriptome and methylome profiling enhances actionable target discovery in high-risk pediatric cancer. Nat Med. 2020;26(11):1742–53.
2. van Tilburg CM, Pfaff E, Pajtler KW, Langenberg KPS, Fiesel P, Jones BC, et al. The Pediatric Precision Oncology INFORM Registry: clinical outcome and benefit for patients with very high-evidence targets. Cancer Discov. 2021;11(11):2764–79.
3. Downing JR, Wilson RK, Zhang J, Mardis ER, Pui CH, Ding L, et al. The Pediatric Cancer Genome Project. Nat Genet. 2012;44(6):619–22.
4. Expanding the reach of anti-PD-1 therapy. Cancer Discov. 2015;5(7):684–5.
5. Vinay DS, Ryan EP, Pawelec G, Talib WH, Stagg J, Elkord E, et al. Immune evasion in cancer: mechanistic basis and therapeutic strategies. Semin Cancer Biol. 2015;35(Suppl):S185–98.
6. Rotte A. Combination of CTLA-4 and PD-1 blockers for treatment of cancer. J Exp Clin Cancer Res. 2019;38(1):255.
7. Schumacher TN, Schreiber RD. Neoantigens in cancer immunotherapy. Science. 2015;348(6230):69–74.
8. Yusko E, Vignali M, Wilson RK, Mardis ER, Hodi FS, Horak C, et al. Association of tumor microenvironment T-cell repertoire and mutational load with clinical outcome after sequential checkpoint blockade in melanoma. Cancer Immunol Res. 2019;7(3):458–65.
9. Pollack SM, He Q, Yearley JH, Emerson R, Vignali M, Zhang Y, et al. T-cell infiltration and clonality correlate with programmed cell death protein 1 and programmed death-ligand 1 expression in patients with soft tissue sarcomas. Cancer. 2017;123(17):3291–304.
10. Terry RL, Meyran D, Ziegler DS, Haber M, Ekert PG, Trapani JA, et al. Immune profiling of pediatric solid tumors. J Clin Invest. 2020;130(7):3391–402.
11. Geoerger B, Kang HJ, Yalon-Oren M, Marshall LV, Vezina C, Pappo A, et al. Pembrolizumab in paediatric patients with advanced melanoma or a PD-L1-positive, advanced, relapsed, or refractory solid tumour or lymphoma (KEYNOTE-051): interim analysis of an open-label, single-arm, phase 1–2 trial. Lancet Oncol. 2020;21(1):121–33.
12. Geoerger B, Zwaan CM, Marshall LV, Michon J, Bourdeaut F, Casanova M, et al. Atezolizumab for children and young adults with previously treated solid tumours, non-Hodgkin lymphoma, and Hodgkin lymphoma (iMATRIX): a multicentre phase 1–2 study. Lancet Oncol. 2020;21(1):134–44.
13. Balar AV, Castellano D, O'Donnell PH, Grivas P, Vuky J, Powles T, et al. First-line pembrolizumab in cisplatin-ineligible patients with locally advanced and unresectable or metastatic urothelial cancer (KEYNOTE-052): a multicentre, single-arm, phase 2 study. Lancet Oncol. 2017;18(11):1483–92.
14. Sadeghi Rad H, Bazaz SR, Monkman J, EbrahimiWarkiani M, Rezaei N, O'Byrne K, et al. The evolving landscape of predictive biomarkers in immuno-oncology with a focus on spatial technologies. Clin Transl Immunol. 2020;9(11):e1215.
15. Galon J, Bruni D. Approaches to treat immune hot, altered and cold tumours with combination immunotherapies. Nat Rev Drug Discov. 2019;18(3):197–218.
16 Cristescu R, Mogg R, Ayers M, Albright A, Murphy E, Yearley J, et al. Pan-tumor genomic biomarkers for PD-1 checkpoint blockade-based immunotherapy. Science. 2018;362(6411):eaar3593.
17. Ott PA, Bang YJ, Piha-Paul SA, Razak ARA, Bennouna J, Soria JC, et al. T-cell-inflamed gene-expression profile, programmed death ligand 1 expression, and tumor mutational burden predict efficacy in patients treated with pembrolizumab across 20 cancers: KEYNOTE-028. J Clin Oncol. 2019;37(4):318–27.
18. Ayers M, Lunceford J, Nebozhyn M, Murphy E, Loboda A, Kaufman DR, et al. IFN-gamma-related mRNA profile predicts clinical response to PD-1 blockade. J Clin Invest. 2017;127(8):2930–40.
19. Danaher P, Warren S, Lu R, Samayoa J, Sullivan A, Pekker I, et al. Pan-cancer adaptive immune resistance as defined by the tumor inflammation signature (TIS): results from The Cancer Genome Atlas (TCGA). J Immunother Cancer. 2018;6(1):63.
20. Newman AM, Liu CL, Green MR, Gentles AJ, Feng W, Xu Y, et al. Robust enumeration of cell subsets from tissue expression profiles. Nat Methods. 2015;12(5):453–7.
21. Newman AM, Steen CB, Liu CL, Gentles AJ, Chaudhuri AA, Scherer F, et al. Determining cell type abundance and expression from bulk tissues with digital cytometry. Nat Biotechnol. 2019;37(7):773–82.
22. Finotello F, Mayer C, Plattner C, Laschober G, Rieder D, Hackl H, et al. Molecular and pharmacological modulators of the tumor immune contexture revealed by deconvolution of RNA-seq data. Genome Med. 2019;11(1):34.
23. Becht E, Giraldo NA, Lacroix L, Buttard B, Elarouci N, Petitprez F, et al. Estimating the population abundance of tissue-infiltrating immune and stromal cell populations using gene expression. Genome Biol. 2016;17(1):218.
24. Jin H, Wan YW, Liu Z. Comprehensive evaluation of RNA-seq quantification methods for linearity. BMC Bioinformatics. 2017;18(Suppl 4):117.
25. Das A, Sudhaman S, Morgenstern D, Coblentz A, Chung J, Stone SC, et al. Genomic predictors of response to PD-1 inhibition in children with germline DNA replication repair deficiency. Nat Med. 2022;28(1):125–35.
26. Grobner SN, Worst BC, Weischenfeldt J, Buchhalter I, Kleinheinz K, Rudneva VA, et al. The landscape of genomic alterations across childhood cancers. Nature. 2018;555(7696):321–7.
27. Aoki T, Hino M, Koh K, Kyushiki M, Kishimoto H, Arakawa Y, et al. Low Frequency of programmed death ligand 1 expression in pediatric cancers. Pediatr Blood Cancer. 2016;63(8):1461–4.
28. Wedekind MF, Denton NL, Chen CY, Cripe TP. Pediatric cancer immunotherapy: opportunities and challenges. Paediatr Drugs. 2018;20(5):395–408.
29. Lau LMS, Mayoh C, Xie J, Barahona P, MacKenzie KL, Wong M, et al. In vitro and in vivo drug screens of tumor cells identify novel therapies for high-risk child cancer. EMBO Mol Med. 2022;14(4):e14608.
30. Patro R, Duggal G, Love MI, Irizarry RA, Kingsford C. Salmon provides fast and bias-aware quantification of transcript expression. Nat Methods. 2017;14(4):417–9.
31. Saletta F, Vilain RE, Gupta AK, Nagabushan S, Yuksel A, Catchpoole D, et al. Programmed death-ligand 1 expression in a large cohort of pediatric patients with solid tumor and association with clinicopathologic features in neuroblastoma. JCO Precis Oncol. 2017;1:1–12.
32. Bankhead P, Loughrey MB, Fernandez JA, Dombrowski Y, McArt DG, Dunne PD, et al. QuPath: open source software for digital pathology image analysis. Sci Rep. 2017;7(1):16878.
33. Cesano A. nCounter® PanCancer Immune Profiling Panel (NanoString Technologies Inc, Seattle, WA). J Immunother Cancer. 2015;3:42.
34. Kuhn M. Building predictive models in R using the caret package. J Stat Softw. 2008;28.
35. Liaw A, Wiener M. Classification and regression by randomForest. R News. 2002;2(3):18–22.
36. Bolotin DA, Poslavsky S, Mitrophanov I, Shugay M, Mamedov IZ, Putintseva EV, et al. MiXCR: software for comprehensive adaptive immunity profiling. Nat Methods. 2015;12(5):380–1.
37. Szolek A, Schubert B, Mohr C, Sturm M, Feldhahn M, Kohlbacher O. OptiType: precision HLA typing from next-generation sequencing data. Bioinformatics. 2014;30(23):3310–6.
38. Weese D, Holtgrewe M, Reinert K. RazerS 3: faster, fully sensitive read mapping. Bioinformatics. 2012;28(20):2592–9.
39. Hundal J, Carreno BM, Petti AA, Linette GP, Griffith OL, Mardis ER, et al. pVAC-Seq: a genome-guided in silico approach to identifying tumor neoantigens. Genome Med. 2016;8(1):11.
40. Karosiene E, Lundegaard C, Lund O, Nielsen M. NetMHCcons: a consensus method for the major histocompatibility complex class I predictions. Immunogenetics. 2012;64(3):177–86.

41. Combes AJ, Samad B, Tsui J, Chew NW, Yan P, Reeder GC, et al. Discovering dominant tumor immune archetypes in a pan-cancer census. Cell. 2022;185(1):184-203 e19.
42. Wargo JA, Reuben A, Cooper ZA, Oh KS, Sullivan RJ. Immune effects of chemotherapy, radiation, and targeted therapy and opportunities for combination with immunotherapy. Semin Oncol. 2015;42(4):601–16.
43. Urso K, Alfranca A, Martínez-Martínez S, Escolano A, Ortega I, Rodríguez A, et al. NFATc3 regulates the transcription of genes involved in T-cell activation and angiogenesis. Blood. 2011;118(3):795–803.
44. Ephrem A, Epstein AL, Stephens GL, Thornton AM, Glass D, Shevach EM. Modulation of Treg cells/T effector function by GITR signaling is context-dependent. Eur J Immunol. 2013;43(9):2421–9.
45. Lalle G, Twardowski J, Grinberg-Bleyer Y. NF-κB in cancer immunity: friend or foe? Cells. 2021;10(2):355.
46. Krummel MF, Allison JP. CD28 and CTLA-4 have opposing effects on the response of T cells to stimulation. J Exp Med. 1995;182(2):459–65.
47. Walunas TL, Lenschow DJ, Bakker CY, Linsley PS, Freeman GJ, Green JM, et al. CTLA-4 can function as a negative regulator of T cell activation. Immunity. 1994;1(5):405–13.
48. Tanaka A, Sakaguchi S. Regulatory T cells in cancer immunotherapy. Cell Res. 2017;27(1):109–18.
49 Alessi M-C, Cenac N, Si-Tahar M, Riteau B. FPR2: a novel promising target for the treatment of influenza. Front Microbiol. 2017;8:1719.
50. Davis AE 3rd, Mejia P, Lu F. Biological activities of C1 inhibitor. Mol Immunol. 2008;45(16):4057–63.
51. House IG, Savas P, Lai J, Chen AXY, Oliver AJ, Teo ZL, et al. Macrophage-derived CXCL9 and CXCL10 are required for antitumor immune responses following immune checkpoint blockade. Clin Cancer Res. 2020;26(2):487–504.
52. Jongbloed SL, Kassianos AJ, McDonald KJ, Clark GJ, Ju X, Angel CE, et al. Human CD141+ (BDCA-3)+ dendritic cells (DCs) represent a unique myeloid DC subset that cross-presents necrotic cell antigens. J Exp Med. 2010;207(6):1247–60.
53. El Kasmi KC, Smith AM, Williams L, Neale G, Panopoulos AD, Watowich SS, et al. Cutting edge: a transcriptional repressor and corepressor induced by the STAT3-regulated anti-inflammatory signaling pathway. J Immunol. 2007;179(11):7215–9.
54 Zhou W-T, Jin W-L. B7–H3/CD276: an emerging cancer immunotherapy. Front Immunol. 2021;12:701006.
55. Lin GL, Nagaraja S, Filbin MG, Suva ML, Vogel H, Monje M. Non-inflammatory tumor microenvironment of diffuse intrinsic pontine glioma. Acta Neuropathol Commun. 2018;6(1):51.
56. Plant AS, Koyama S, Sinai C, Solomon IH, Griffin GK, Ligon KL, et al. Immunophenotyping of pediatric brain tumors: correlating immune infiltrate with histology, mutational load, and survival and assessing clonal T cell response. J Neurooncol. 2018;137(2):269–78.
57. Li B, Li T, Pignon JC, Wang B, Wang J, Shukla SA, et al. Landscape of tumor-infiltrating T cell repertoire of human cancers. Nat Genet. 2016;48(7):725–32.
58. van Tilburg CM, Witt R, Heiss M, Pajtler KW, Plass C, Poschke I, et al. INFORM2 NivEnt: the first trial of the INFORM2 biomarker driven phase I/II trial series: the combination of nivolumab and entinostat in children and adolescents with refractory high-risk malignancies. BMC Cancer. 2020;20(1):523.
59. Hutchison S, Pritchard AL. Identifying neoantigens for use in immunotherapy. Mamm Genome. 2018;29(11–12):714–30.
60. Duan F, Duitama J, Al Seesi S, Ayres CM, Corcelli SA, Pawashe AP, et al. Genomic and bioinformatic profiling of mutational neoepitopes reveals new rules to predict anticancer immunogenicity. J Exp Med. 2014;211(11):2231–48.
61. Davis KL, Fox E, Reid JM, Liu X, Minard CG, Weigel B, et al. ADVL1412: initial results of a phase I/II study of nivolumab and ipilimumab in pediatric patients with relapsed/refractory solid tumors—a COG study. Am Soc Clin Oncol. 2017;35(15_suppl):10526.
62. Merchant MS, Wright M, Baird K, Wexler LH, Rodriguez-Galindo C, Bernstein D, et al. Phase I clinical trial of ipilimumab in pediatric patients with advanced solid tumors. Clin Cancer Res. 2016;22(6):1364–70.
63. Forrest SJ, Al-Ibraheemi A, Doan D, Ward A, Clinton CM, Putra J, et al. Genomic and immunologic characterization of INI1-deficient pediatric cancers. Clin Cancer Res. 2020;26(12):2882–90.
64. Jacobs J, Deschoolmeester V, Zwaenepoel K, Rolfo C, Silence K, Rottey S, et al. CD70: an emerging target in cancer immunotherapy. Pharmacol Ther. 2015;155:1–10.
65. Draghi A, Chamberlain CA, Khan S, Papp K, Lauss M, Soraggi S, et al. Rapid identification of the tumor-specific reactive TIL repertoire via combined detection of CD137, TNF, and IFNγ, following recognition of autologous tumor-antigens. Front Immunol. 2021;12:705422.
66. Savas P, Virassamy B, Ye C, Salim A, Mintoff CP, Caramia F, et al. Single-cell profiling of breast cancer T cells reveals a tissue-resident memory subset associated with improved prognosis. Nat Med. 2018;24(7):986–93.
67. Solinas C, Aiello M, Rozali E, Lambertini M, Willard-Gallo K, Migliori E. Programmed cell death-ligand 2: a neglected but important target in the immune response to cancer? Transl Oncol. 2020;13(10):100811.
68. Chen S, Crabill GA, Pritchard TS, McMiller TL, Wei P, Pardoll DM, et al. Mechanisms regulating PD-L1 expression on tumor and immune cells. J Immunother Cancer. 2019;7(1):305.
69. Nicola NA, Babon JJ. Leukemia inhibitory factor (LIF). Cytokine Growth Factor Rev. 2015;26(5):533–44.
70. Pascual-Garcia M, Bonfill-Teixidor E, Planas-Rigol E, Rubio-Perez C, Iurlaro R, Arias A, et al. LIF regulates CXCL9 in tumor-associated macrophages and prevents CD8(+) T cell tumor-infiltration impairing anti-PD1 therapy. Nat Commun. 2019;10(1):2416.
71. Wong M, Mayoh C, Lau LMS, Khuong-Quang DA, Pinese M, Kumar A, et al. Whole genome, transcriptome and methylome profiling enhances actionable target discovery in high-risk pediatric cancer. EGAS00001004572, EGA. 2020. https://ega-archive.org/studies/EGAS00001004572.
72. Mayoh C, Gifford AJ, Terry R, Lau LMS, Wong M, Rao P, et al. A novel transcriptional signature identifies T-cell infiltration in high-risk paediatric cancer. EGAS00001007029, EGA. 2023. https://ega-archive.org/studies/EGAS00001007029.
73. Mayoh C, Gifford AJ, Terry R, Lau LMS, Wong M, Rao P, et al. A novel transcriptional signature identifies T-cell infiltration in high-risk paediatric cancer. Github. 2023. https://github.com/CCICB/iPASS/.

Publisher's Note